Comparison of Scan Strategies for Side Roughness Optimization of Al6061-Zr Alloy Produced by Laser Powder Bed Fusion (L-PBF), benefits and Drawbacks on Different Part Profiles

M. Beal[1,a,*]

[1]University of Lyon, Ecole Centrale de Lyon - ENISE, Laboratoire de Tribologie et Dynamique des Systèmes, CNRS UMR 5513, 58 rue Jean Parot, 42023 Saint-Etienne, France

[a]maxime.beal@enise.fr

Abstract. Laser Powder Bed Fusion (L-PBF) is an additive manufacturing process that allows to build parts by solidifying powder bed, layer by layer, with a laser. This approach offers the possibility to build complex geometries. However, due to the succession of layers, the use of powder as raw material and melt pool dynamic, the surface roughness generated through this process is a limitation for some applications. Several works have been conducted to improve surface roughness by improving scan strategies such as contouring, and compensation optimization. However, these improvements are mostly applied on usual materials and on simple geometries. The aim of this work was i) to compare roughness obtained on cubes with high performance aluminium alloy (6061-Zr) and cast alloy (AlSi7Mg), ii) apply roughness optimization strategy on 6061-Zr on cubes and iii) compare typical L-PBF geometries obtained with and without roughness optimization strategies. This study shows that LPBF using Al6061-Zr alloy produces a higher roughness than AlSi7Mg (+16 %). The strategies used allowed the roughness to be reduced (-63 %) as well as obtaining a better circularity and a more homogeneous surface. It was also shown that some strategies have weaknesses for specific geometrical shapes.

Introduction

Laser Powder Bed Fusion (L-PBF) as known as Selective Laser Melting (SLM) is an additive manufacturing process that allows to build near net shape parts layer by layer by solidifying a powder bed with a laser. Complex structures can be printed with this process. The Al6061-Zr has a very good thermal conductivity, good corrosion resistance and it is suitable for hard anodizing [1]. The first aluminium alloys investigated with the L-PBF process were mainly cast alloys [2]. However, as the technology became more mature and more widely used in industry, cast alloys showed limitations. Trials were then carried out with the 6XXX and 7XXX ranges which have better thermal and mechanical properties [3]. Nevertheless, these alloys show a high sensitivity to hot cracking during the L-PBF process. This phenomenon has already been highlighted in the welding process [4] and has been investigated in additive manufacturing more recently [3]. Zirconium has been added during the gas atomization to avoid hot cracking [3,5]. However, even though this modification allows the alloy to be built via L-PBF, the mechanical properties of the "as built" parts are impacted by the roughness of the process. Obtaining a good surface finish is essential for certain applications, to prevent cracking initiation and avoid premature failure [6]. Work has already been carried out to improve the roughness of the parts produced by L-PBF processes by adjusting the build parameters [7] (power, speed, hatch distance, layer thickness) and the laser strategies (optimization of compensation [8], contours [6,8–10]).

The aim of this study is to observe the difference in roughness between the cast alloys and an alloy from the 6XXX range without a roughness optimization strategy. Secondly, the roughness optimization strategies from the literature will be applied and optimized to the 6XXX alloy. Finally, the final part consists of applying these optimized strategies to geometries that are widely present in the construction of parts by L-PBF process because most of the works carried out today are applied only to cubes.

Experimental

Material. Aluminium alloy 6061 powder was used in this study whose main chemical elements are Silicon (Si) and Magnesium (Mg). However, the silicon content of this alloy is much lower than the silicon content of cast aluminium alloys (AlSi12Mg, AlSi10Mg, AlSi7Mg). In order to avoid hot cracking, Zirconium element has been added during the gas atomization of the powder. The composition of the alloy used in our study was developed by Thales. The studied alloy will be referred as 6061-Zr in the present work. The size distribution of the power ranged from 5 to 65 µm. The L-PBF equipment used in this study is a 3DSystems® ProX200 machine. The employed laser is a Yb-fiber machine with a spot diameter of 150 µm delivering a maximum power output of 300W. The maximum power (300 W) and a laser speed of 2200 mm/s were used to print the samples under an argon atmosphere. The recovery rate was set at 50 % and the layer thickness at 30 µm. These parameters will be referred as "raw parameters" in this study. These are the process parameters that give the best density and productivity without applying a roughness optimization strategy.

Method & surface characterization. The study is divided into three parts. First of all, 3 cubes have been printed in 6061-Zr with the raw parameters. These cubes are oriented in such a way as to minimize the material fronts facing the coating roller (45° rotation around z-axis). The four side faces of the three cubes are analyzed to highlight any dispersal between the cubes (repeatability) and check a potential difference in roughness between the "North-West" (NW), "North-East" (NE), "South-East" (SE) and "South-West" (SW) faces (see Fig. 1).
Secondly, the next two roughness optimization strategies will be applied and optimized for the material 6061-Zr on cubes:
- "Compensation strategy": The compensations consist in defining a distance during which the mirrors reach their nominal speed to print in the expected conditions. The software developed by 3DSYSTEMs® enables to adjust the start and end compensation values. . Inspired by the work of Masiagutova et al. [8], a delta (Δ) has been introduced: Δ=start-stop. The start compensation was left fixed and the stop compensation was modified to observe the effect of this variation and its impact on the roughness of the manufactured parts.
- "Contour strategy" [6,8–10]: to avoid the start and end of single tracks which can deteriorate the surface roughness by running a track along the CAD file while covering the hatching. This strategy has been subdivided into two strategies: "Contour before" filling and "contour after" filling. Different contour scan speeds are tested to obtain the best roughness. The offset between the contours and the filling has been optimized to avoid the formation of porosity due to lack of fusion [11].

The best results of each strategy will be retained in the third part of this study. The last part of the present work consists of comparing the roughness and form of printed parts according to the strategies used. The geometry of the printed parts is based on the geometry commonly found in L-PBF process:
- sloping surfaces from 0° (vertical) to 75°
- cylinders
- non supported holes
- lattices

A 3D mapping of the surfaces is acquired using a focus variation microscope (Alicona Infinite Focus). From this mapping, the *Sa* value is measured (arithmetical mean height of a surface). As the roughness of the L-PBF parts is quite coarse, the mapping was done using a magnification of x5. The vertical resolution was set at 500 nm and the lateral resolution at 5 µm. "Plane" form removal was applied to cubes, cylinders and inclined surfaces before extracting surface roughness values. No further filters were used for the roughness.

Result and Discussion

Raw. The three cubes printed with the raw parameters, without roughness optimization method have a similar roughness as shown in Fig. 1. This allows to conclude that the generated roughness during the process seems repeatable over several parts. Fig. 1 also shows the impact of the cube orientation on the roughness. We can see that, except the "North East" face, the surfaces have similar roughness. In some works, we find a fairly good stability as in our study [12], whereas some authors show a significant difference between the faces [8,13].
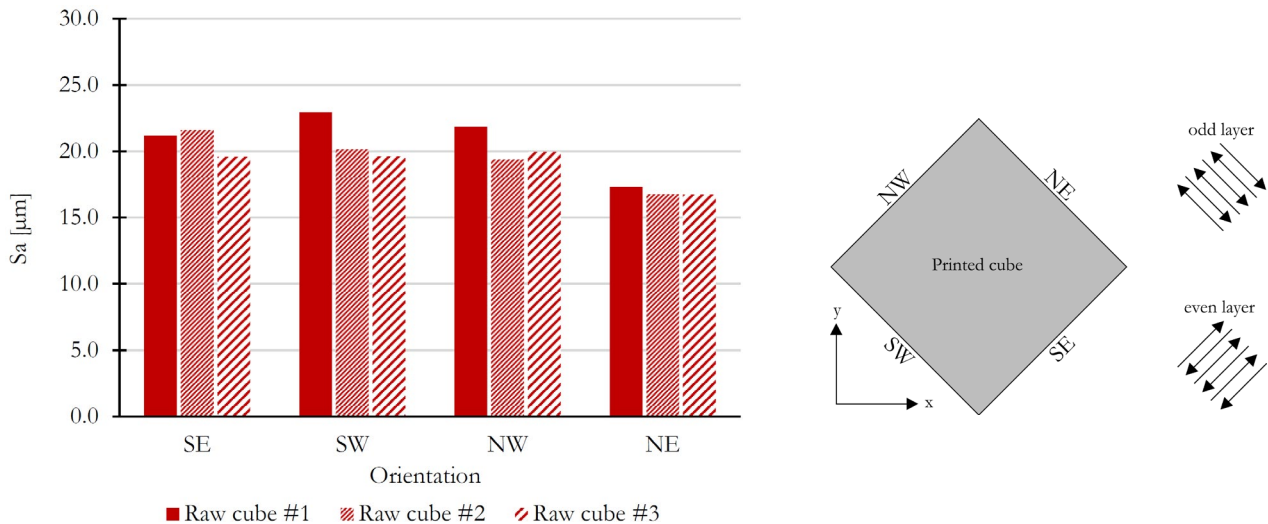
Fig. 1: Roughness repeatability and impact of orientation

The roughness of the four faces was averaged to give the overall vertical roughness of the cubes. The vertical roughness obtained for the 6061-Zr is Sa = 19.8 µm. This roughness value is compared to the mean value obtained on identical cubes with an AlSi7 alloy. This alloy is more suitable for the L-PBF process than 6061 even though its Si content is lower than AlSi10 or AlSi12. Therefore, we can assume that its roughness may be better. The Fig. 2 below shows the difference in vertical roughness between the AlSi7 alloy with Sa = 17.0 µm and the 6061-Zr alloy with Sa = 19.8 µm. The roughness obtained with 6061-Zr is 16% higher. This difference could potentially be larger because the favorable parametric window for AlSi7 is large, which makes it possible to optimize the roughness while maintaining a good density [8,13,14]. Bhaduri & Al. [14] reduced the lateral roughness from more than 20 µm to 13.6 on AlSi10Mg. In this study, the parameters used for the construction of AlSi7 are the parameters giving the best productivity, which does not necessarily correspond to the best roughness. Unlike AlSi7, 6061-Zr has a restricted favorable parametric window and does not allow the optimization of roughness while guaranteeing the density of parts. In the literature, Majeed & Al. [12] as well as Kamarudin & Al. [7] achieve a lateral roughness below 5 µm with AlSi10Mg. These results cannot be directly compared with the values obtained in this work because the roughness depends on many factors such as the machine used, the powder, the parameters employed. Nevertheless, the results obtained with AlSi10Mg are significantly lower than those obtained with 6061-Zr. A low silicon content disturbs the printability of the material despite the addition of zirconium (Zr).

Sa = 17.0 μm   Sa = 19.8 μm

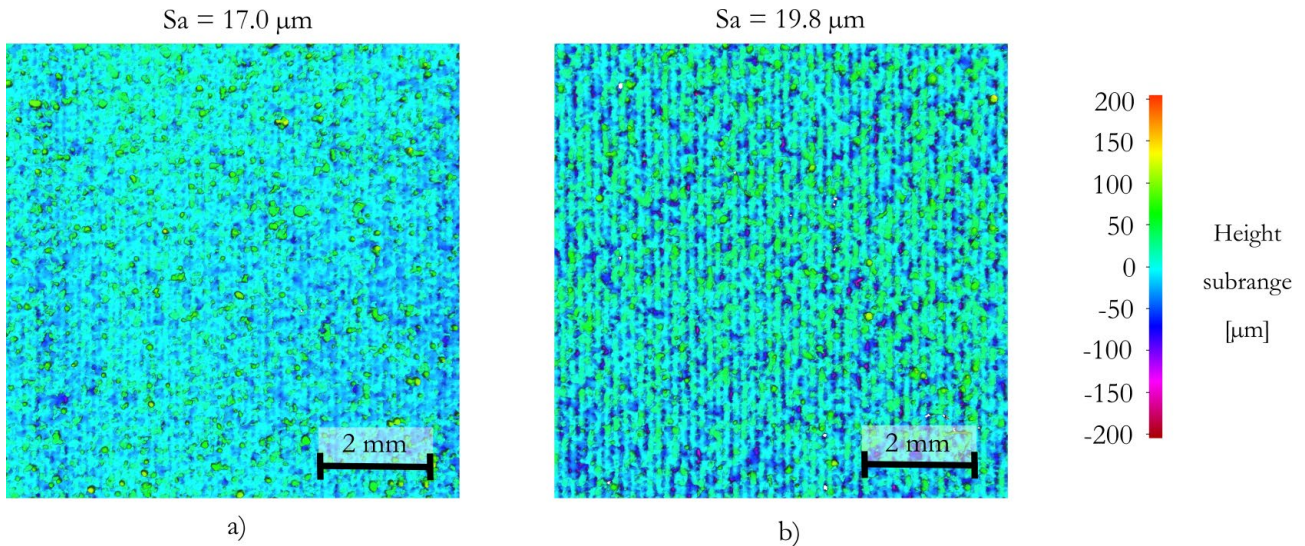a)   b)

Fig. 2: Surface mapping of AlSi7Mg (a) and 6061-Zr (b)

In Fig. 2, it can be noticed that the roughness profile seems different. Indeed, the roughness of surface (Fig. 2-a) appears to be mainly related to the presence of satellites and partially melted particles. As for surface (Fig. 2-a), the roughness defect of 6061-Zr surface (Fig. 2-b) seems to come from the presence of satellites and partially melted particles but also from the juxtaposition of the single tracks which is more pronounced.

Compensation method. The work presented by Masiagutova & Al. [8] shows that the vertical roughness is linearly related to the compensation delta. They worked on a range of delta from -140 μm up to +140 μm. In this range of variation, it was witnessed a decrease of factor 5 of the roughness dropping from 50 μm to 11μm. As a reminder the *delta* value is the difference between the *start* and *stop*, Fig. 3 shows a schematic illustration of different delta values
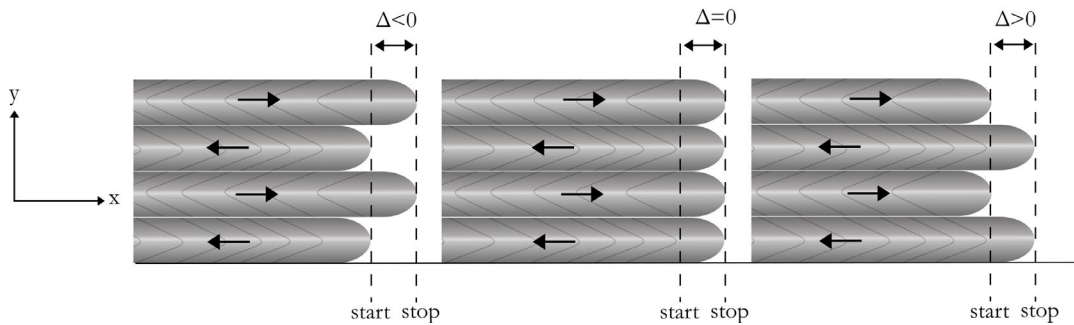

Fig. 3: Schematic illustration of compensation values impact

In this study, the delta value is tested from -180 to +440 μm as positive delta values seem to give the best results [8]. Fig. 4 highlights the evolution of *Sa* compared to the *delta* value. We can observe two levels, one level where the roughness is around 40μm for delta lower than 100 μm and a second level from a *delta* of 40μm where the roughness is around 20 μm. From a delta of -100 μm to 40 μm, it can be witnessed a decrease of the surface roughness. In our case, the roughness is only governed by the sign of delta and not its value (Fig. 5-a). The linear behavior between the two stages corresponds to the fact that the single tracks are not perfectly constant and can vary more or less in length.
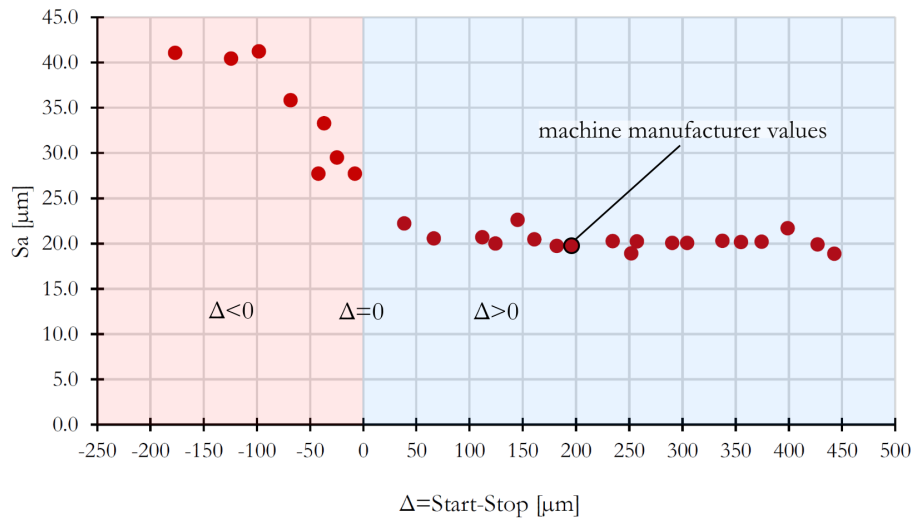
Fig. 4: Impact of Δ value on roughness

This binary is probably related to the overlap rate between each single track. Indeed, the optimal parameters for processing the 6061-Zr alloy consists in recovering each single track at 50% unlike the work of Majeed & Al. with AlSi10Mg alloy where the recovery rate varies from 25 to 35% [12]. The high overlap used for 6061-Zr is responsible for the binary of the result. Indeed, Fig. 5 shows that with a 50% overlap, the generated surface is either governed by the beginning of the single tracks or by the end. This is in contrast to Fig. 5-b. where the recovery rate is lower than 50% as used in the work of Masiagutova & Al. and Majeed & Al [15]. We can conclude that this optimizing method is only valid for parameters where the recovery rate is strictly less than 50%. We can assume that the lower is the recovery rate value, the higher will be the impact of optimizing the compensation value.
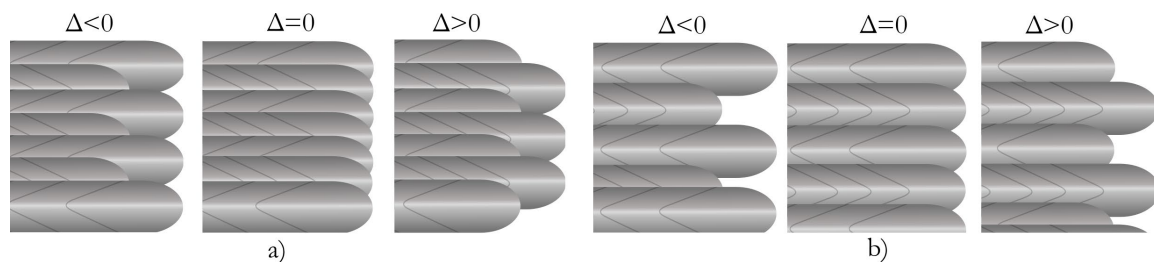

Fig. 5: Schematic illustration of the effect of delta on roughness for recovery rate ≥ 50 % (a) and recovery rate < 50 % (b)

Considering that the generated surfaces are produced only by the beginning or the end of the single tracks and that negative delta values produce a roughness higher than positive delta values, we can conclude that the end of the tracks generates a more degraded surface than the beginning of the tracks.

Contour method. Concerning the "contour after bulk" strategy, the basic reasoning was to "clean" the lateral surface by having the laser to re-melt the partially fused particles, the defects, without attracting new particles [16]. For this purpose, volume energy densities similar to "raw" parameters energy were employed. Different offsets and speeds were tested (from 1600 mm/s to 2800 mm/s). However, all samples had to be cancelled due to excessive friction between the coating roller and the constructions. It was concluded that "cleaning" the surface was not suitable in our case. The second method is to re-melt the material to create a stable melt pool around the part with lower lasering speeds (from 400 mm/s to 1300 mm/s).

For the "contour before bulk" strategy, only low speeds are used (from 400 mm/s to 1300 mm/s) as it is necessary to create a stable bead around the part in a blank powder bed. In fact, contrary to filling, there is no energy accumulation making the speed used in the "raw" parameter too fast.

Fig. 6 shows the results of the contour before (Fig. 6-a) and contour after (Fig. 6-b). The parts built with a contour with a scan speed of 400 mm/s were cancelled due to an excess of energy and instability. The best results are obtained with a speed of 700mm/s for both contour strategies. The

roughness obtained at this speed is Sa = 7.4 µm for both contour strategies. When the speed increases (1000 and 1300 mm/s) the strategy "Contour before" filling guarantees an improvement of the roughness with a *Sa* of about 12 µm. At 1000 mm/s, the strategy "Contour after" improves the roughness to approximately 15µm. At 1300 mm/s it produces a surface with a *Sa* value similar to the one obtained without the optimization strategy (Sa ≈ 20 µm).

a)   b)
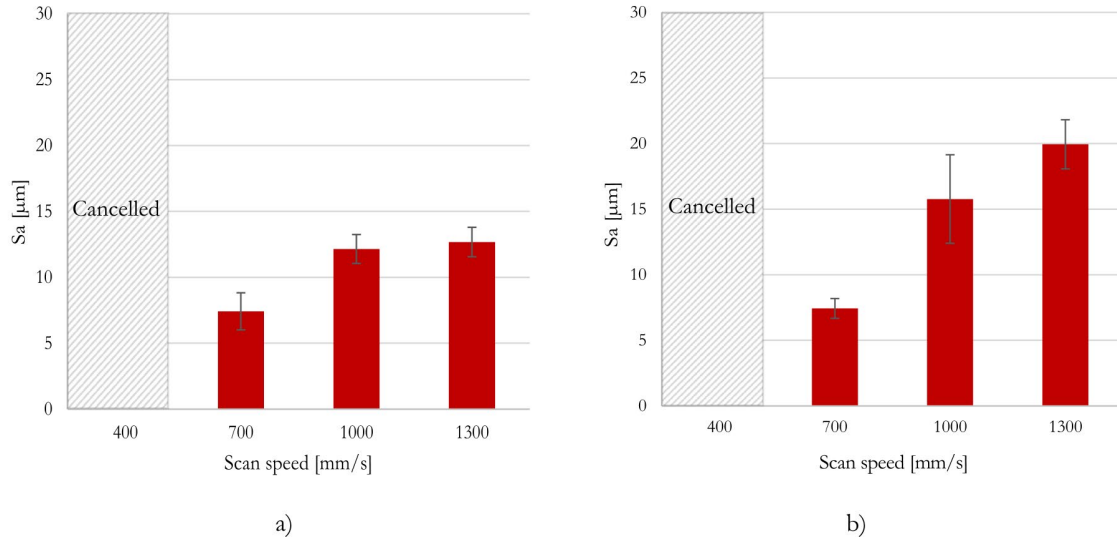
Fig. 6: Influence of contour method before feeding (a) and contour after feeding (b) on roughness

However, spherical pores were observed in the contours produced at low speeds. This phenomenon concerns the speed of 700 mm/s and 1000mm/s for the contour strategy before filling and only V = 700 mm/s for the contour strategy after filling. For this paper, contours with a speed of 700 mm/s are chosen for both strategies. Nevertheless, higher speeds are also chosen to avoid spherical pores. For the strategy contour after filling, the speed of 1000 mm/s is chosen because it does not present spherical pores. Parts built with the contour after fill strategy at 700 mm/s will be called "contour after low speed″ and those at 1000 mm/s will be called "contour after high speed". The contour before filling strategy generates spherical pores for speeds of 700 mm/s and 1000mm/s, but at 1300mm/s, the generated melt pool is too thin to make the optimization of the offset between contour and filling. Either the offset is too high and pores of the lack of fusion type are present at the contour/fill interface, or the offset is too low and the melt pool "overflows" from the contour annihilating the benefits of the contour. Therefore, only the speed of 700 mm/s is used for the contour strategy before the fill. Parts built using this roughness optimization strategy will be named "contour before".

Application of roughness optimization strategies on typical L-PBF geometries
Parametric optimization strategies have been applied and optimized for 6061-Zr alloy. These strategies are tested on geometries that are often found in parts manufactured by the L-PBF process. The results are compared to the same parts without any particular strategy (raw).

Sloping surfaces. All inclined surfaces were successfully manufactured (from 0° to 75°). The Fig.7 below shows a schematic representation of the inclined surfaces, the upskin and downskin faces are indicated on the scheme.
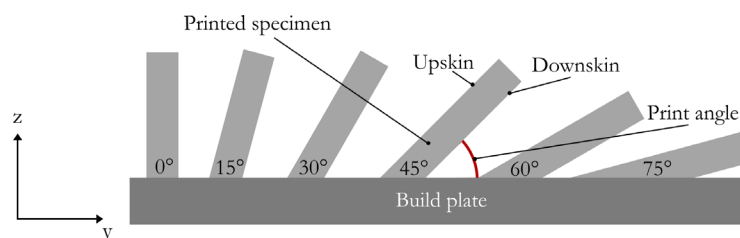

Fig. 7: Schematic illustration of sloped surfaces

The roughness values of the Raw sample at 0° are lower than previously presented (Fig. 2). This difference is due to the orientation of the lasering with respect to the orientation of the part. When the cubes were printed, they were oriented at 45° along the construction axis (z) and the lasering is also carried out at 45°. When printing inclined planes, the specimens are not oriented at 45°. The difference in orientation between the laser path and the part has an impact on the roughness for specimens without contours. This variation can create a heterogeneous surface on a part compared to the contour strategy.
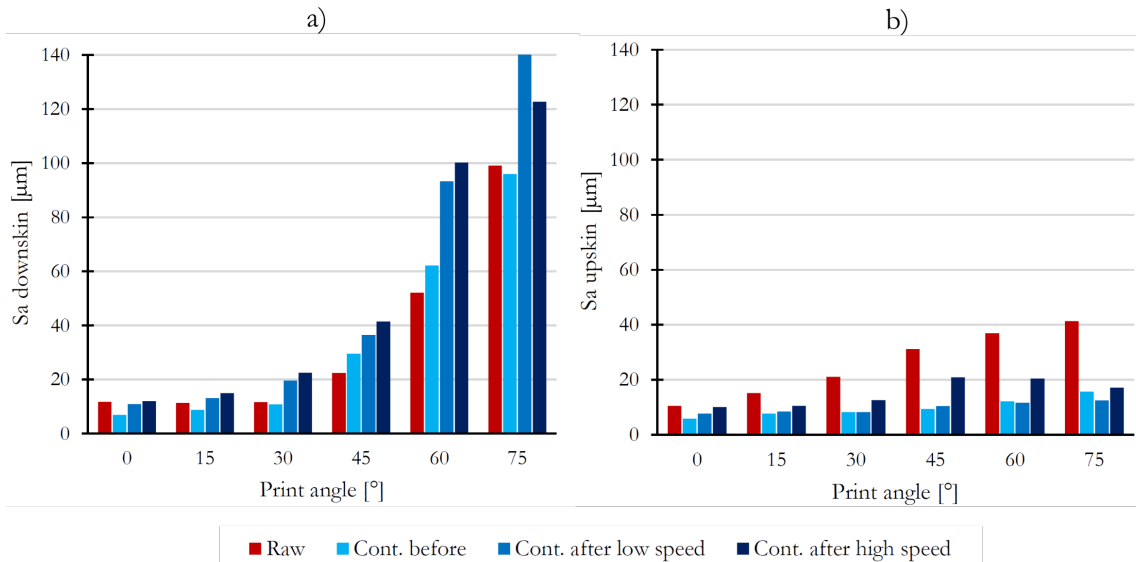

Fig. 8: Effect of angle on downskin (a) and upskin (b) roughness

Fig. 8-a highlights that the increase in roughness of downskin surfaces as a function of part inclination is exponential. The roughness of the "contour after" specimens increases from 30° of inclination whereas the Raw and "contour before" specimens are stable until 45° where the roughness increases for all specimens. After 45°, the Raw and contour before strategies generate less chaotic surfaces than the contour after samples, however the roughness is higher than 50μm. For the upskin surfaces, the low speed contour strategies ("Contour before" and "Contour after lowspeed") provide a good surface finish despite a slight degradation. Indeed, at 60° their respective Sa are 12.2 μm and 11.6 μm. The samples printed without any optimization strategy show a strong degradation of the surface finish as a function of the tilt angle. At 60°, the *Sa* is approximately 37 μm. Finally, the "contour after high speed" strategy does not provide as good a surface as the "low speed" ones but the roughness is less than 20 μm up to 60°. Fig. 9 below shows the average radius of the 4 corners of the vertical pieces. The "contour before" and "contour after low speed" strategies have the largest radius. The raw sample has the smallest radius in spite of the angle between the manufactured part and the lasering angle. It is possible that the radius is even smaller when the orientation of the lasering and the part are similar.
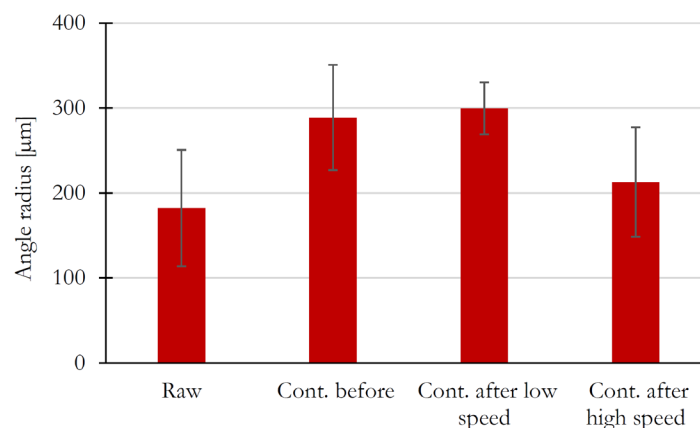

Fig. 9: Impact of roughness optimization strategies on angle radius of parallelepiped

Cylinders. On cylinders, the optimization strategies have a strong impact. Fig. 10 shows the roughness in the (X,Y) plane. The row cylinder has a roughness of about 20 µm except for three areas circled in blue where Sa is about 10µm. These three areas correspond to the case where the angle between the surface and the orientation of the laser is 45° as for inclined surfaces. These favorable areas are narrow and are less representative than the rougher surface. We consider the "normal" surface as the roughness of 20µm.
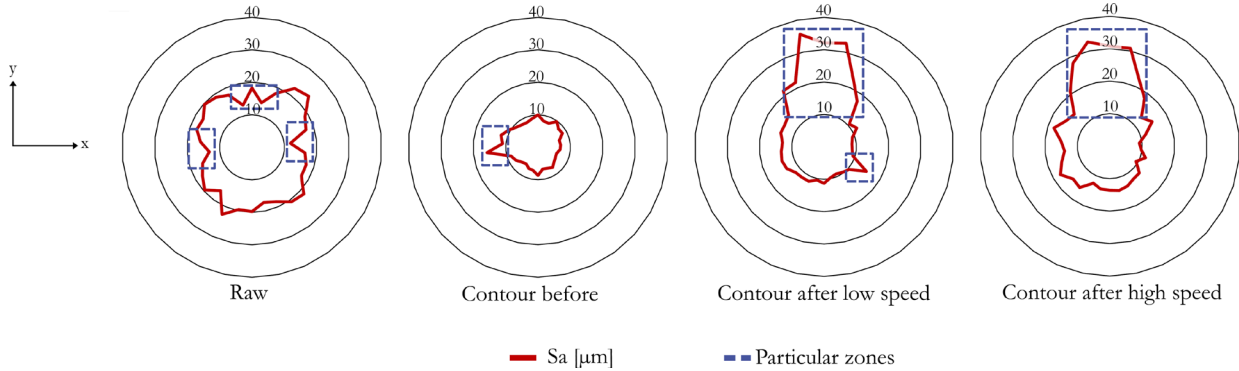

Fig. 10: Cylinder roughness projected on the (X,Y) plane and particular zones

Fig. 11 shows the particular areas previously highlighted by blue rectangles in Fig.10. It can be seen on the "raw" cylinder that these areas are visible and appear smooth. The "contour before" cylinder has a roughness of less than 10 µm around almost the entire cylinder. A local increase in roughness is noticeable. Figure 11 highlights this particular area which represents the overlap area between the start and end of the contour. This zone is also found on the "contour after low speed" cylinder, which has a roughness slightly greater than 10 µm, except in this recovery zone and on the section following y+, where it can be seen in Fig. 11 that numerous projections are present. The "contour after high speed" cylinder has the same projections oriented in the same way. It seems that the "contour after" method is responsible for the accumulation of satellites on the face following y+.
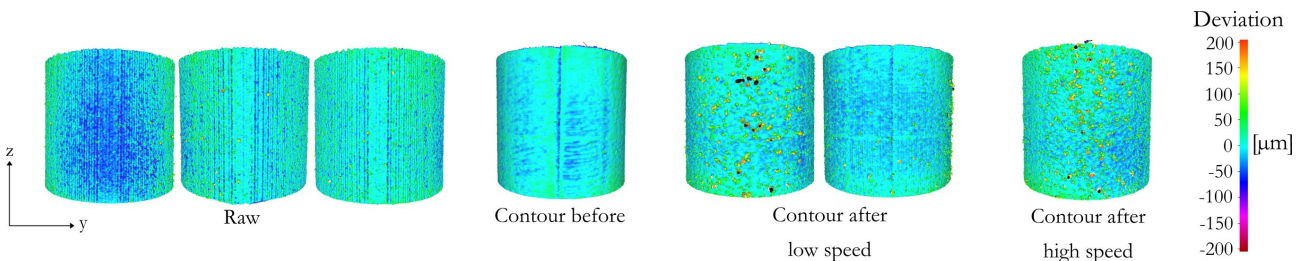

Fig. 11: 3D mapping of particular zones on cylinders

Regarding the shape, it is observable that the raw cylinder does not really look cylindrical. In order to perceive more easily the circularity defects, a section was made along the XY plane and the difference between the real diameter and the equivalent diameter calculated thanks to the least squares is plotted in Fig. 12. This gap is filtered with a low pass filter at 800 µm to highlight the shape defects. As analyzed earlier, it can be seen that the contour before cylinder is relatively cylindrical. In addition to the satellites located on one side of the cylinder, the cylinder printed with the "contour after low speed" strategy is also quite cylindrical. On the other hand, the raw and contour after high speed cylinder has a particular butterfly shape.
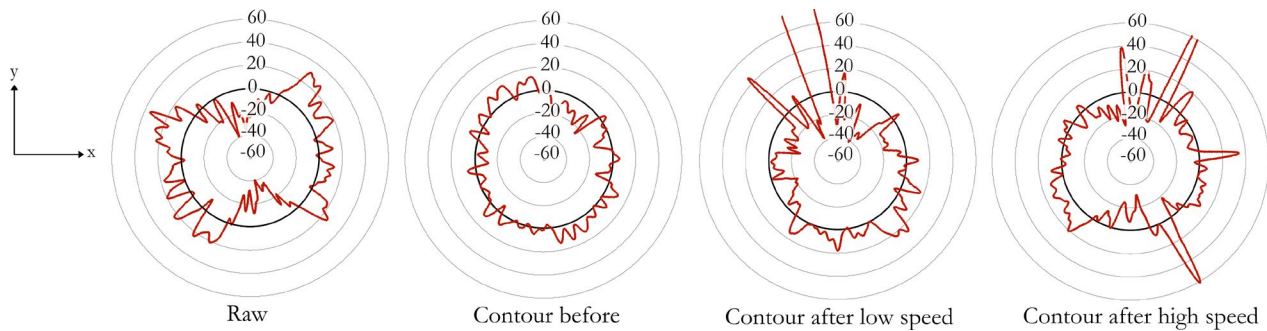
Fig. 12: Deviation projected on the (X,Y) plane between real and equivalent diameter calculated with least squares (filtered with Lc = 800 µm)

However, it is difficult to draw conclusions from a single cut of the cylinders. For this purpose, the criteria RONa, RONp and RONv are introduced as shown in Fig. 13 below. RONa is the mean of the absolute radial deviations to a least squares circle, RONp is the maximum peak to reference roundness deviation and RONv is the maximum reference to valley roundness deviation. It is observable that the "contour before" cylinder presents the best RONa which corresponds to the best circularity. Concerning RONp, the two cylinders built with the "contour after" strategy show a higher value because of the projections present on the cylinder. The RONv is slightly lower for the cylinder having been built with the "contour before" strategy.
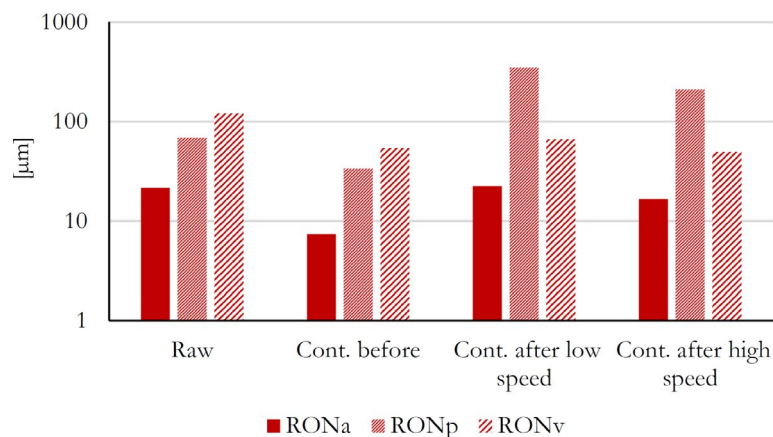

Fig. 13: Effect of roughness optimization strategies on shape defect

Holes. To observe the form defects of the holes, a 2D profile averaged over 600 µm is extracted from the 3D mapping. This averaging results in a loss of roughness information but allows a better observation of the shape defects. The profiles obtained with the four strategies are shown in Fig. 14-a. We can observe that the "raw" strategy shows little sagging in contrast to the other strategies, especially "contour after low speed" which shows a strong sagging. Nevertheless, the profiles from the raw and contour after high speed strategies show a misalignment with the theoretical profile. The "contour before" and "contour after low speed" strategies do not show any misalignment. The histogram Fig. 14-b shows the difference in the area under the curve of the real profile and the theoretical profile. It can be seen that, as discussed visually, the profile from the "raw" strategy has the best fit and the "contour after low speed" strategy has the worst. The "contour before" and "contour after high speed" strategies have a similar defect however "contour before" is preferable because of its alignment with the theoretical profile.
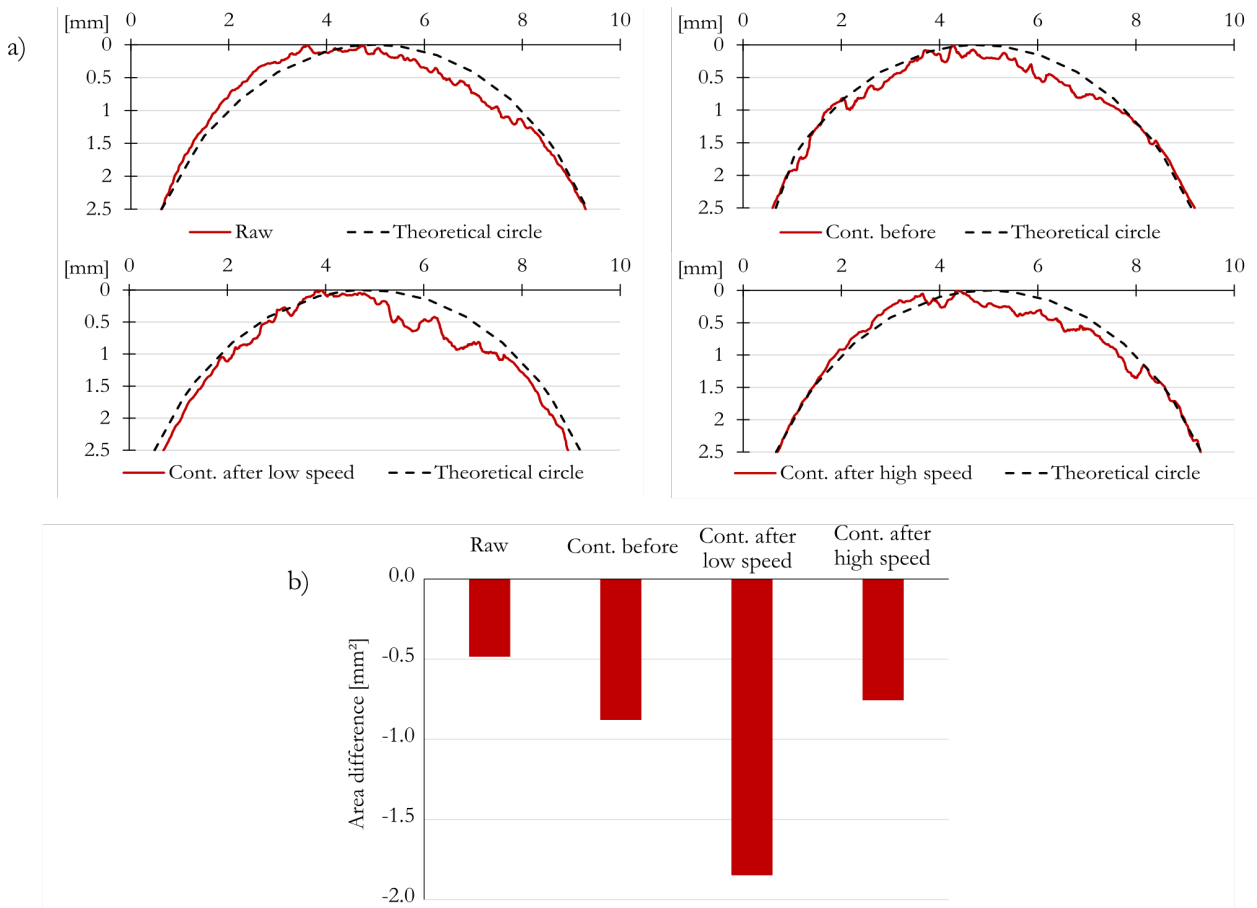
Fig. 14: 2D profile of holes (a) and area difference between theoretical and real profile (b)

Lattices structures. The lattice structures show an impressive density to strength ratio. This strength is strongly influenced by the type of lattice structure used [15]. In this work, the printed structure is the BCC (Body centered cubic unit cell) which is the least efficient but the easiest to print. The printed cells are 7x7mm with a theoretical branch diameter of 0.5 mm. It can be observed on Fig. 15 that the "contour after" methods do not allow the print of lattice structures because some branches are broken. The lattice structures printed in raw and with the "contour before" strategy are whole and seem to be well printed. It can be observed that the roughness of the lattice structure printed with the "contour before" strategy seems to be better than the "raw" but the roughness on the lower part of the branches is very degraded as illustrated in the work of Leary & Al. [15] and in Fig.15.
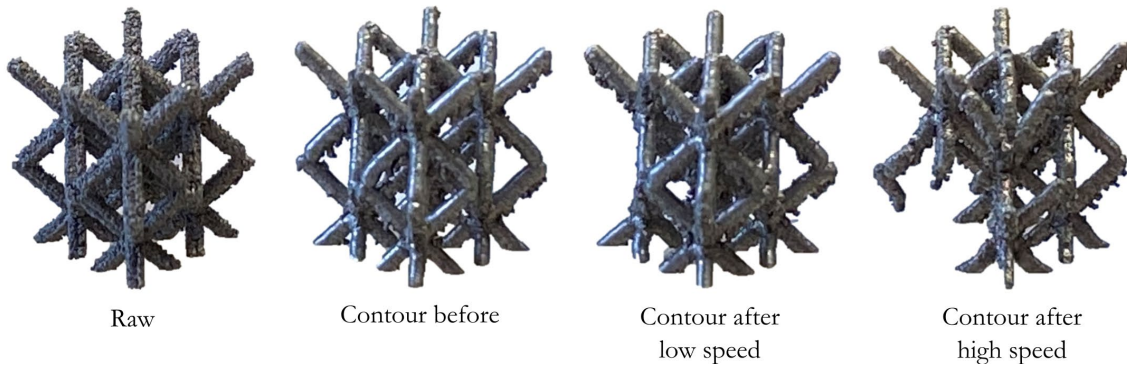

Fig. 15: Printed lattices structures

Conclusion

In the present paper, the roughness optimization of 6061-Zr alloy has been studied. We observed that 6061-Zr has a 16% higher roughness than AlSi7Mg. The compensation strategy did not improve surface quality due to a recovery rate over 50 %. The "contour before" and "contour after" strategies resulted in a significant reduction in roughness value. A Sa of 7.4 µm has been reached for the "contour before" strategy at a laser speed of 700 mm/s. Nevertheless, the contour strategies showed the presence of pores at low speed (700 mm/s). In order to avoid porosity, higher contour lasering speed (1000 mm/s) has been investigated for the "contour after filling" strategy.

Parts with more complex geometries were printed raw and with the three strategies "contour before" and "contour after low speed" with a scan speed of 700 mm/s, and "contour after high speed" at 1000 mm/s.

- Regarding sloped surfaces, the best roughness value for downskin surfaces is obtained with the two low speed strategies "Contour before" and "Contour after lowspeed". Nevertheless, the roughness value increases exponentially for all strategies over 45°. The two low speed strategies also produce the best results for upskin surfaces. At 60° their respective Sa are 12.2 µm and 11.6 µm which is three times lower than the "raw" specimen. The "Contour after highspeed" strategy also shows an improvement over the "raw" specimen but less than the low speed strategies ("Contour before" & "Contour after lowspeed"). As for the "raw" specimen, it presents the highest roughness value with a Sa at 60° exceeding 25 µm. For the angle radius, the strategies using the contour lower the sharpness of the corners, the part built without optimization strategy shows the best result with an average radius of 182 µm.

- For cylinders, the "Contour before" strategy gives the best roughness. Furthermore, the roughness is homogeneous over the entire surface of the cylinder apart from the contour overlap. This overlap could be optimized in the future to increase the homogeneity of the roughness. This strategy also offers the best circularity.

- About the holes, the raw specimen gives the smallest delta of area between real and theoretical profile. However, the profile generated by the raw strategy is misaligned with the CAD profile. The 'Contours before' do not show any misalignment but the sagging is very marked

- The lattice structures built without an optimisation strategy (raw) show a high visual but homogeneous roughness. The "contour before" strategy shows visually a better surface condition but more irregular with particles fused to the surface of the downskin parts. The "contour after" strategies do not allow the construction of lattice structures.

Finally, the optimization strategy with the most advantages is the "Contour before" strategy. In order to limit the sagging of unsupported surfaces, it could be interesting to disable the contour on these areas. Author would recommend to perform fatigue tests on specimens printed without strategy (raw) and with "contour before" and "contour after" with scan speed of 700 mm/s. This study could allow to observe if it is more critical to generate spherical pores in the skin of the part but with a good surface finish or a rough surface but without internal defects.

References

[1] A.K. Lakshminarayanan, V. Balasubramanian, K. Elangovan, Effect of welding processes on tensile properties of AA6061 aluminium alloy joints, Int. J. Adv. Manuf. Technol. 40 (2009) 286–296. https://doi.org/10.1007/s00170-007-1325-0.

[2] N.T. Aboulkhair, M. Simonelli, L. Parry, I. Ashcroft, C. Tuck, R. Hague, 3D printing of Aluminium alloys : Additive Manufacturing of Aluminium alloys using selective laser melting, Prog. Mater. Sci. 106 (2019) 1–45. https://doi.org/10.1016/j.pmatsci.2019.100578.

[3] J.H. Martin, B.D. Yahata, J.M. Hundley, J.A. Mayer, T.A. Schaedler, T.M. Pollock, 3D printing of high-strength aluminium alloys, Nat. Publ. Gr. 549 (2017) 365–369. https://doi.org/10.1038/nature23894.

[4]   C.E. Cross, On the origin of weld solidification cracking, Hot Crack. Phenom. Welds. (2005) 3–18. https://doi.org/10.1007/3-540-27460-X_1.

[5]   H. Zhang, H. Zhu, X. Nie, J. Yin, Z. Hu, X. Zeng, Effect of Zirconium addition on crack, microstructure and mechanical behavior of selective laser melted Al-Cu-Mg alloy, Scr. Mater. 134 (2017) 6–10. https://doi.org/10.1016/j.scriptamat.2017.02.036.

[6]   Y. Tian, D. Tomus, P. Rometsch, X. Wu, Influences of processing parameters on surface roughness of Hastelloy X produced by selective laser melting, Addit. Manuf. 13 (2017) 103–112. https://doi.org/10.1016/j.addma.2016.10.010.

[7]   K. Kamarudin, M.S. Wahab, A.A. Raus, A. Ahmed, S. Shamsudin, Benchmarking of dimensional accuracy and surface roughness for AlSi10Mg part by selective laser melting (SLM), AIP Conf. Proc. 1831 (2017). https://doi.org/10.1063/1.4981188.

[8]   E. Masiagutova, F. Cabanettes, A. Sova, M. Cici, G. Bidron, P. Bertrand, Side surface topography generation during laser powder bed fusion of AlSi10Mg, Addit. Manuf. 47 (2021) 102230. https://doi.org/10.1016/j.addma.2021.102230.

[9]   T. Yang, T. Liu, W. Liao, E. MacDonald, H. Wei, X. Chen, L. Jiang, The influence of process parameters on vertical surface roughness of the AlSi10Mg parts fabricated by selective laser melting, J. Mater. Process. Technol. 266 (2019) 26–36. https://doi.org/10.1016/j.jmatprotec.2018.10.015.

[10]   O. Poncelet, M. Marteleur, C. van der Rest, O. Rigo, J. Adrien, S. Dancette, P.J. Jacques, A. Simar, Critical assessment of the impact of process parameters on vertical roughness and hardness of thin walls of AlSi10Mg processed by laser powder bed fusion, Addit. Manuf. 38 (2021) 101801. https://doi.org/10.1016/j.addma.2020.101801.

[11]   P. Karimi, C. Schnur, E. Sadeghi, J. Andersson, Contour design to improve topographical and microstructural characteristics of Alloy 718 manufactured by electron beam-powder bed fusion technique, Addit. Manuf. 32 (2020) 101014. https://doi.org/10.1016/j.addma.2019.101014.

[12]   A. Majeed, A. Ahmed, A. Salam, M.Z. Sheikh, Surface quality improvement by parameters analysis, optimization and heat treatment of AlSi10Mg parts manufactured by SLM additive manufacturing, Int. J. Light. Mater. Manuf. 2 (2019) 288–295. https://doi.org/10.1016/j.ijlmm.2019.08.001.

[13]   F. Calignano, D. Manfredi, E.P. Ambrosio, L. Iuliano, P. Fino, Influence of process parameters on surface roughness of aluminum parts produced by DMLS, Int. J. Adv. Manuf. Technol. 67 (2013) 2743–2751. https://doi.org/10.1007/s00170-012-4688-9.

[14]   D. Bhaduri, P. Penchev, S. Dimov, K. Essa, L.N. Carter, C.I. Pruncu, J. Jiang, D. Pullini, On the surface integrity of additive manufactured and post-processed AlSi10Mg parts, Procedia CIRP. 87 (2020) 339–344. https://doi.org/10.1016/j.procir.2020.02.093.

[15]   M. Leary, M. Mazur, J. Elambasseril, M. McMillan, T. Chirent, Y. Sun, M. Qian, M. Easton, M. Brandt, Selective laser melting (SLM) of AlSi12Mg lattice structures, Mater. Des. 98 (2016) 344–357. https://doi.org/10.1016/j.matdes.2016.02.127.

[16]   T. Yang, T. Liu, W. Liao, E. MacDonald, H. Wei, X. Chen, L. Jiang, The influence of process parameters on vertical surface roughness of the AlSi10Mg parts fabricated by selective laser melting, J. Mater. Process. Technol. 266 (2019) 26–36. https://doi.org/10.1016/j.jmatprotec.2018.10.015.